GPS Solut
DOI 10.1007/s10291-013-0331-y

ORIGINAL ARTICLE

Forward modeling of GPS multipath for near-surface reflectometry and positioning applications

Felipe G. Nievinski · Kristine M. Larson

Received: 9 October 2012 / Accepted: 3 June 2013

Abstract Multipath is detrimental for both GPS positioning and timing applications. However, the benefits of GPS multipath for reflectometry have become increasingly clear for soil moisture, snow depth, and vegetation growth monitoring. Most multipath forward models focus on the code modulation, adopting arbitrary values for the reflection power, phase, and delay, or they calculate the reflection delay based on a given geometry and keep reflection power empirically defined. Here, a fully polarimetric forward model is presented, accounting for right- and left-handed circularly polarized components of the GPS broadcast signal and of the antenna and surface responses as well. Starting from the fundamental direct and reflected voltages, we have defined the interferometric and error voltages, which are of more interest in reflectometry and positioning applications. We examined the effect of varying coherence on signal-to-noise ratio, carrier phase, and code pseudorange observables. The main features of the forward model are subsequently illustrated as they relate to the broadcast signal, reflector height, random surface roughness, surface material, antenna pattern, and antenna orientation. We demonstrated how the antenna orientation—upright, tipped, or upside-down—involves a number of trade-offs regarding the neglect of the antenna gain pattern, the minimization of CDMA self-interference, and the maximization of the number of satellites visible. The forward model was also used to understand the multipath signature in GPS positioning applications. For example, we have shown how geodetic GPS antennas offer little impediment for the intake of near-grazing reflections off natural surfaces, in contrast to off metal, because of the lack of diversity with respect to the direct signal—small interferometric delay and Doppler, same sense of polarization, and similar direction of arrival.

Keywords GPS · GNSS · Multipath · Reflectometry · Reflections · Interferometric · Coherent · Simulator · Simulation

F. G. Nievinski (✉) · K. M. Larson
Department of Aerospace Engineering Sciences, University of Colorado Boulder, Boulder, CO 80309-0429, USA
e-mail: fgnievinski@gmail.com

Introduction

For GPS users, multipath is used to describe the combined reception of direct or line-of-sight (LOS) signals and reflections, diffractions, or scatterings thereof. Multipath is detrimental for both GPS positioning and timing applications. However, the benefits of GPS multipath for reflectometry have become increasingly clear in the last decade. Specifically, the frequencies and amplitudes of the multipath signal observed in GPS data show strong correlations with environmental characteristics such as soil moisture, snow depth, and vegetation growth (Larson et al. 2008, 2009; Rodriguez-Alvarez et al. 2011a; Small et al. 2010).

Most multipath forward models focus on the code modulation, adopting arbitrary values for the reflection power, phase, and delay, or they calculate the reflection delay based on a given geometry and keep reflection power empirically defined. Here, a fully polarimetric forward model is presented, accounting for right- and left-handed circularly polarized components of the GPS broadcast signal and of the antenna and surface responses as well. It is based on the model developed by Zavorotny et al. (2010); it has been extended to allow for variable incident power and polarization, antenna orientation, code pseudorange, and noise power. The provision of a polarimetric

Published online: 25 June 2013

formulation is expected to foster its adoption for those assessing multipath effects in positioning solutions and serve as a platform for further research in GPS reflectometry.

In the next section, we will describe each of the components of the forward model. We conclude with simulations in various reflection situations. An accompanying follow-on paper, to appear in the GPS Toolbox column, will describe the software simulator, as well as review the relevant literature.

Formulation

We start by introducing direct and reflected signals, based upon which we define the interferometric and error quantities. The former two signals are more basic or fundamental, while the latter two quantities are of main interest in reflectometry and positioning applications. We proceed to expose the effect of varying coherency on power and phase. Then, we examine the code modulation impressed on the carrier wave, with special consideration for multipath or composite-signal reception. We characterize the antenna response in terms of its complex vector effective length, which dictates how the propagating electric field is transformed into a circuit current. The direct and reflected fields are subsequently detailed. The noise power spectral density and bandwidth are defined, and with it the signal-to-noise ratio. We end with a summary of the expressions developed.

Interferometric and error quantities

Let the direct voltage, collected at the satellite line of sight, be $V_\mathrm{d} = |V_\mathrm{d}| \exp(\imath\phi_\mathrm{d})$, with its time-dependent magnitude $|V_\mathrm{d}|$ and phase ϕ_d (with the imaginary unity denoted $\imath = \sqrt{-1}$). The reflection voltage is V_r. Their complex ratio

$$V_\mathrm{i} = V_\mathrm{r}/V_\mathrm{d} \tag{1}$$

is called the interferometric voltage, and it is the main quantity of interest for coherent reflectometry applications. The interferometric phase, $\phi_\mathrm{i} = \phi_\mathrm{r} - \phi_\mathrm{d}$, amounts to the reflection excess phase with respect to the direct one. The interferometric power, $P_\mathrm{i} = |V_\mathrm{i}|^2 = P_\mathrm{r}/P_\mathrm{d}$, isolates the reflectivity by which the medium responds independently from the directly collected power.

In positioning applications, the reciprocal of interferometric power is known as "D/U", the desired-to-undesired power ratio. The complex sum of direct and reflection voltages

$$V_\mathrm{c} = V_\mathrm{r} + V_\mathrm{d} = V_\mathrm{d}(1 + V_\mathrm{i}) = V_\mathrm{d}V_\mathrm{e} \tag{2}$$

is the composite voltage. The composite phase, ϕ_c, just like the reflection phase ϕ_r, is contaminated by the direct phase, ϕ_d, which contains many unknown terms (clocks, atmospheric delays, etc.); this makes it difficult to use them for reflection studies. The ratio of composite to direct voltages

$$V_\mathrm{e} = V_\mathrm{c}/V_\mathrm{d} = 1 + V_\mathrm{i} \tag{3}$$

will be called the error voltage. It is the main quantity of interest for positioning applications because its phase $\phi_\mathrm{e} = \phi_\mathrm{c} - \phi_\mathrm{d}$ quantifies how much phase tracking is in error compared to the assumption of reflection-free or direct-only conditions, i.e., $\phi_\mathrm{c} = \phi_\mathrm{d} + \phi_\mathrm{e}$.

Interferometric and error phases are reckoned from the direct phase, and they can be related as:

$$\phi_\mathrm{e} = \mathrm{Atan}(\sqrt{P_\mathrm{i}} \sin\phi_\mathrm{i}, 1 + \sqrt{P_\mathrm{i}} \cos\phi_\mathrm{i}) \tag{4}$$

where $\mathrm{Atan}(\cdot,\cdot)$ is the two-argument four-quadrant arc-tangent; it computes the principal value of the argument function applied to an equivalent complex number, $\mathrm{Atan}(y,x) = \arg(x + \imath y)$ and simplifies to the ordinary arc-tangent in the first quadrant of the complex plane, $\mathrm{Atan}(y,x) = \mathrm{atan}(y/x), x > 0$. Assuming $P_\mathrm{r} \ll P_\mathrm{d}$:

$$\phi_\mathrm{e} \approx \sqrt{P_\mathrm{i}} \sin\phi_\mathrm{i} = \mathrm{Im}\{V_\mathrm{i}\} \tag{5}$$

(in radians). So the error phase ϕ_e would seem to be more difficult to model accurately than the interferometric phase ϕ_i, because the former depends additionally on the interferometric power P_i. The corresponding (coherent) powers are related as

$$P_\mathrm{e} = 1 + P_\mathrm{i} + 2\sqrt{P_\mathrm{i}} \cos\phi_\mathrm{i}, \tag{6}$$

$$P_\mathrm{c} = P_\mathrm{d} + P_\mathrm{r} + 2\sqrt{P_\mathrm{d}}\sqrt{P_\mathrm{r}} \cos\phi_\mathrm{i}. \tag{7}$$

In contrast to direct, reflected, and interferometric powers, the error power P_e and the composite power $P_\mathrm{c} = P_\mathrm{d}P_\mathrm{e}$ both include a trigonometric term.

This same nomenclature will be used for the propagation delays as well: τ_d (direct), τ_r (reflected), $\tau_\mathrm{i} = \tau_\mathrm{r} - \tau_\mathrm{d}$ (interferometric), $\tau_\mathrm{c} = \tau_\mathrm{d} + \tau_\mathrm{e}$ (composite), and τ_e (error). There is no such a thing as a composite propagation path, so the composite delay cannot be defined in terms of ray properties; rather, it is to be interpreted as the delay by which a signal replica needs to be shifted, such that is maximizes the correlation with the measured composite signal (see below for details). The delay multipath error in general depends on the particular code discriminator employed by the receiver (several are implemented in our simulator), although approximations exist to circumvent it; details are given below.

Coherence

The composite power $P_\mathrm{c} = |V_\mathrm{c}|^2 = |V_\mathrm{d} + V_\mathrm{r}|^2$ should be considered in the average sense:

$$\langle P_c \rangle = \langle V_d^* V_d \rangle + \langle V_r^* V_r \rangle + \langle V_d^* V_r \rangle + \langle V_r^* V_d \rangle \quad (8)$$

where * is complex conjugation and the brackets $\langle \cdot \rangle$ denote statistical expectation. It is convenient to express it in terms of the complex-valued coherence, $\gamma \equiv \langle V_d^* V_r \rangle / \sqrt{\langle V_d^* V_d \rangle \langle V_r^* V_r \rangle}$:

$$\langle P_c \rangle = \langle P_d \rangle + \langle P_r \rangle + 2\sqrt{\langle P_d \rangle}\sqrt{\langle P_r \rangle}|\gamma| \cos \phi_\gamma \quad (9)$$

The polar decomposition, $\gamma = |\gamma| \exp(\imath \phi_\gamma)$, is especially insightful. Assuming the direct signal to be deterministic causes it to cancel out of the coherence power (squared degree of coherence),

$$|\gamma|^2 = |\langle V_r \rangle|^2 / \left\langle |V_r|^2 \right\rangle \quad (10)$$

which can then be interpreted as a measure of the reflection phase purity or variance; the deterministic direct signal remains only in the coherence argument,

$$\phi_\gamma = \arg(\langle V_r \rangle) - \arg(\langle V_d \rangle) \quad (11)$$

which is nothing but the interferometric phase, ϕ_i.

Further decomposing the reflection voltage into two components, $V_r = V_r^I + V_r^C$, the incoherent component is defined such that its complex product $V_r^I V$ is zero on average for voltages other than itself, $V \neq V_r^I$, because its phase $\arg(V_r^I)$ is random (yet, its average power P_r^I remains nonzero). In contrast, the coherent component has its average power equal simply to the power implied by its average voltage, $\left\langle |V_r^C|^2 \right\rangle = |\langle V_r^C \rangle|^2 = \langle P_r^C \rangle$. Thus, only the coherent component survives in the average reflection voltage, $\langle V_r \rangle = \langle V_r^C \rangle$, but both components are present in the average reflection power, $\langle P_r \rangle = \langle P_r^I \rangle + \langle P_r^C \rangle$.

The coherence phase $\phi_\gamma = \arg(\langle V_r \rangle) - \arg(\langle V_d^C \rangle)$ then involves only the coherent component, and the degree of coherence (squared)

$$|\gamma|^2 = \langle P_r^C \rangle / (\langle P_r^C \rangle + \langle P_r^I \rangle) \quad (12)$$

reveals to be simply the coherent fraction of the total reflected power; a binomial expansion $|\gamma| \approx 1 - 0.5\langle P_r^I \rangle / \langle P_r^C \rangle$ shows further that it decreases with increasing incoherent-to-coherent power ratio (assuming $\langle P_r^C \rangle \gg \langle P_r^I \rangle$). The matching between the scattered power spectral distribution on the one hand and the measurement averaging period on the other hand will dictate what proportion of the total reflected power can be captured coherently—essentially a low-pass filter. For the same physical scattering process, the amount of coherently collected power can be varied employing varying coherent integration periods. The degree of coherence quantifies this gradation in a continuum between 0 and 1.

Substituting the coherent and incoherent powers into the composite power, and dropping the brackets notation, we finally obtain:

$$P_c = P_d + P_r^C + 2\sqrt{P_d}\sqrt{P_r^C} \cos \phi_i + P_r^I = |V_d + V_r^C|^2 + P_r^I \quad (13)$$

The degree of coherence $|\gamma|$ disappears, and we are left with the interference of direct and coherently reflected voltages, in addition to the incoherent reflected power.

Incoherent power

Incoherent reflections are incapable of affecting the expected value of the interferometric phase; however, its variance is affected—as the magnitude of the complex coherence γ diminishes, it becomes more difficult to recover its phase. In forward modeling of GPS multipath observables, neglecting incoherent power P_r^I is inconsequential for carrier phase. SNR is affected, but only in its trend tSNR $\propto P_d + P_r^C + P_r^I$—which is typically a monotone function of elevation angle—over which the interference fringes dSNR $\propto 2\sqrt{P_d}\sqrt{P_r^C} \cos \phi_i$ are superimposed. Finally, the pseudorange can be influenced by P_r^I, depending on the code discriminator employed. We will neglect incoherent power from now on; we will model the coherent reflection only, $V_r = V_r^C$, whose magnitude and phase will incorporate the effects of varying coherence.

Code modulation

The voltages V above are the result of a matching filter that correlates the received voltage Z against a replica Z_0 of the transmitted signal over a given coherent integration time T:

$$V = \frac{1}{T} \int_{-T/2}^{+T/2} Z^* Z_0(t)\, dt \quad (14)$$

The replica $Z_0(t) = C(t - \tau_0) \exp(\imath 2\pi f_0 t)$ mimics the code modulation C and carrier frequency f impressed on received voltage $Z = YC(\tau) \exp(\imath 2\pi f t)$. The post-correlation result can be expressed as $V = YW\Psi$, where the pre-correlation voltage Y is described below. The unity complex factor $\Psi = \exp(\imath 2\pi(\delta\tau + \delta f T))$ accounts for an out-of-lock phase change. The real-valued Woodward ambiguity function $W \approx \Lambda\Gamma$ can be separated into two factors, a product of the code auto-correlation $\Lambda(\delta\tau)$ (function of delay difference $\delta\tau = \tau_0 - \tau$ and the code chipping rate) and a normalized sinc function $\Gamma(\delta f) = \mathrm{sinc}(\delta f T) = \sin(\pi \delta f T)/(\pi \delta f T)$ (dependent on the frequency difference $\delta f = f_0 - f$ accumulated coherently during T). This separability applies to BPSK modulations

(Zavorotny and Voronovich 2000), as utilized in all legacy GPS signals, as well as in the newer L2C signal and the newest L5 signal; it will not fully hold for the future GPS L1C signal, whose design is based on a BOC modulation.

In the case of multipath reception, the matching is done using a single replica against the composite voltage. In this case, the replica is locked such that $\Psi = 1$. The direct and reflection delay tracking differences are, respectively,

$$\delta\tau_\mathrm{d} = \tau_0 - \tau_\mathrm{d} = \tau_\mathrm{e} \tag{15}$$

$$\delta\tau_\mathrm{r} = \tau_0 - \tau_\mathrm{r} = \tau_\mathrm{e} + \tau_\mathrm{d} - \tau_\mathrm{r} = \tau_\mathrm{e} - \tau_\mathrm{i} \tag{16}$$

The corresponding frequency differences are similar, $\delta f_\mathrm{d} = \Delta f_\mathrm{e}$, $\delta f_\mathrm{r} = \delta f_\mathrm{e} - \Delta f_\mathrm{i}$, and in fact are just delay-rates scaled by wavelength, e.g., $\Delta f_\mathrm{i} = \dot{\tau}_\mathrm{i}/\lambda = \Delta f_\mathrm{r} - \Delta f_\mathrm{d}$, where the dot denotes time-derivative. These frequencies are not to be confused with the Doppler shifts experienced by the direct and reflected signals, $\Delta f_\mathrm{d} = \dot{\tau}_\mathrm{d}/\lambda$, $\Delta f_\mathrm{r} = \dot{\tau}_\mathrm{r}/\lambda$, whose absolute value is generally much greater than δf_d, δf_r. The direct and reflected ambiguity functions thus read $W_\mathrm{d} = \Lambda(\tau_\mathrm{e})\Gamma(\Delta f_\mathrm{e})$ and $W_\mathrm{r} = \Lambda(\tau_\mathrm{e} - \tau_\mathrm{i})\Gamma(\Delta f_\mathrm{e} - \Delta f_\mathrm{i})$. Everything else being the same, stationary multipath is more severe than fast-changing multipath, because of the suppression offered by the sinc function Γ.

Given the interferometric delay τ_i and precorrelation direct and reflection voltages Y_d and Y_r, the delay error τ_e can be calculated rigorously employing a code discriminator function against the composite voltage $V_\mathrm{c} = V_\mathrm{d} + V_\mathrm{r} = Y_\mathrm{d}W_\mathrm{d} + Y_\mathrm{r}W_\mathrm{r}$. An initial guess $\tau_\mathrm{e} = 0$ is improved iteratively until convergence, applying the corrections provided by the discriminator. This is akin to what a receiver performs in real time. The Doppler error Δf_e could be obtained via numerical differentiation of a time succession of so-obtained delay errors τ_e. Notice that the interferometric Doppler Δf_i is nonzero even for a stationary receiver and stationary surface, except when the satellite direction is also stationary—it is a consequence of the displacement of the specular point. We will ignore Doppler from now on.

For small interferometric delays, it may be acceptable to neglect code modulation entirely, as the approximation $Y_\mathrm{c} \approx V_\mathrm{d} + V_\mathrm{r}$ is reasonably accurate in terms of the phase error ϕ_e and also composite power P_c. Moreover, in this case, the error delay can be approximated as:

$$\tau_\mathrm{e} \approx \tau_\mathrm{i}\sqrt{P_\mathrm{i}}\cos\phi_\mathrm{i}/(1 + \sqrt{P_\mathrm{i}}\cos\phi_\mathrm{i}) \tag{17}$$

Compounding this small-delay approximation with the previous small-power approximation ($P_\mathrm{i} \ll 1$), we obtain:

$$\tau_\mathrm{e} \approx \tau_\mathrm{i}\mathrm{Re}\{V_\mathrm{i}\} = \tau_\mathrm{i}\sqrt{\left(1 - \phi_\mathrm{e}^2\right)} \tag{18}$$

Later, we will assess the accuracy of these expressions. Such insensitivity of the error delay to any particular code discriminator is helpful for reflectometry applications because environmental retrievals are less likely to be receiver-dependent. This also implies that all receivers are equally bad in mitigating short-delay multipath, which is unfortunate for positioning applications. It is only for large interferometric delays that the code modulation becomes effective in suppressing the reflection voltage V_r, which contributes less and less compared to the direct one V_d, eventually being rejected from the composite voltage V_c as τ_i exceeds a threshold (beyond the code chip width).

Antenna response

The precorrelation voltages Y are scalars that result from the dot-product of a vector-valued electric field $\bar{E} = \left[E^\mathrm{R}, \quad E^\mathrm{L}\right]^\mathrm{T}$ (in terms of right- and left-handed polarization components—RHCP and LHCP) against the antenna complex vector effective length (in meters), thus converting from volts-per-meter to volts (Milligan 2005):

$$Y_\mathrm{d} = \overline{L}_\mathrm{d}^\dagger \overline{E}_\mathrm{d} \tag{19}$$

$$Y_\mathrm{r} = \overline{L}_\mathrm{r}^\dagger \overline{E}_\mathrm{r} \tag{20}$$

where the dagger † denotes conjugate transposition. The subscript serves as shorthand for the direction at which the antenna response is evaluated, e.g., for $\overline{L}_\mathrm{d}$, the direct signal's boresight angle and axial angle in the antenna body-fixed coordinate system.

The vector norm $L = \|\overline{L}\| = \left(|L^\mathrm{R}|^2 + |L^\mathrm{L}|^2\right)^{1/2}$ is given by (Milligan 2005) as

$$L = L_\mathrm{iso}\sqrt{G} \tag{21}$$

The complex effective length of an isotropic antenna is $L_\mathrm{iso} = 2\sqrt{(Z/Z_0)\lambda^2/(4\pi)}$, and the effective area of an isotropic antenna is $\lambda^2/(4\pi)$; Z is the load impedance (in ohms) and Z_0 is the vacuum impedance. The antenna gain G (usually given in decibels, $G = 10\log_{10} G_\mathrm{dB}$)—not to be confused with the peak gain—is direction-dependent but polarization-independent. The polarization dependency is represented by the complex unity vector $\hat{L} = \overline{L}/L$ (notice $\hat{L}^\dagger\hat{L} = 1$):

$$\begin{aligned}\hat{L} &= \left[\hat{L}^\mathrm{R}, \quad \hat{L}^\mathrm{L}\right]^\mathrm{T} \\ &= (1/\sqrt{G})\left[\sqrt{G^\mathrm{R}}\exp\left(\imath\Phi^\mathrm{R}\right), \quad \sqrt{G^\mathrm{L}}\exp\left(\imath\Phi^\mathrm{L}\right)\right]^\mathrm{T}\end{aligned} \tag{22}$$

The magnitudes follow from the respective partial power gains for each RHCP and LHCP (G^R, G^L), and similarly for the total power gain, $G = G^\mathrm{R} + G^\mathrm{L}$; the respective antenna phase patterns are denoted $\Phi^\mathrm{R}, \Phi^\mathrm{L}$. Defining the antenna polarimetric power ratio, $G^{\mathrm{L/R}} = G^\mathrm{L}/G^\mathrm{R}$, as well as the antenna polarimetric phase difference, $\Phi^{\mathrm{L-R}} = \Phi^\mathrm{L} - \Phi^\mathrm{R}$,

we can write the antenna complex vector effective length as:

$$\begin{aligned}\overline{L} &= \left[L^{\mathrm{R}}, \quad L^{\mathrm{L}} \right]^{\mathrm{T}} \\ &= L_{\mathrm{iso}} \sqrt{G^{\mathrm{R}}} \exp\left(-\imath \Phi^{\mathrm{R}}\right) \left[1, \quad \sqrt{G^{\mathrm{L/R}}} \exp\left(-\imath \Phi^{\mathrm{L-R}}\right) \right]^{\mathrm{T}}\end{aligned} \tag{23}$$

(The antenna phases are denoted by uppercase letters, e.g., $\Phi_{\mathrm{d}}^{\mathrm{R}} = \arg\left(L_{\mathrm{d}}^{\mathrm{R}}\right)$, and the electric field phases are lowercase, e.g., $\phi_{\mathrm{d}}^{\mathrm{L}} = \arg\left(E_{\mathrm{d}}^{\mathrm{L}}\right)$; voltage phases are also lowercase, but need no superscript, e.g., $\phi_{\mathrm{r}} = \arg(V_{\mathrm{r}})$, as they have no polarization.)

Antenna gain

The antenna gain pattern, G, for each polarization and as evaluated in each direct and reflected direction $G_{\mathrm{d,r}}^{\mathrm{R,L}}$, can be measured in anechoic chambers. GPS antennas are typically set upright, being omni-directional in azimuth and hemispherical in elevation angle, to allow multiple satellites to be tracked simultaneously while minimizing ground noise reception. Sometimes the antenna is turned upside-down, or tipped with its boresight facing the horizon; see below for discussion. By transforming the viewing direction—from east, north, up coordinates to antenna body-aligned components, arbitrary antenna orientations are reduced to the upright installation case.

Antenna phase

The receiver antenna phase pattern is typically only known in RHCP, Φ^{R}, because this has the greatest impact on positioning applications. It can be modeled as

$$\Phi^{\mathrm{R}} = -\vec{\Phi}^{\mathrm{R}} \cdot \hat{\rho} + \tilde{\Phi}^{\mathrm{R}} \tag{24}$$

The first term consists of the phase center offset, $\vec{\Phi}^{\mathrm{R}} = \left[\Phi_{\mathrm{x}}^{\mathrm{R}}, \Phi_{\mathrm{y}}^{\mathrm{R}}, \Phi_{\mathrm{z}}^{\mathrm{R}}\right]^{\mathrm{T}}$ (a spatial vector, $\vec{\Phi} \in \mathbb{R}^3$, not to be confused with EM vectors, $\overline{E} \in \mathbb{C}^2$), projected on the viewing direction, $\hat{\rho}$. The second term $\tilde{\Phi}^{\mathrm{R}}$ is the phase center variation, a scalar-valued function describing the asphericity of the wavefronts generated by an astigmatic antenna; it is of the order of millimeters near the boresight for geodetic-quality antennas. The phase pattern tends to be dominated by a centimeter-level vertical component of the offset vector (assuming an upright installation), $\Phi^{\mathrm{R}} \approx -\Phi_{\mathrm{z}}^{\mathrm{R}} \sin e$. This yields a phase excess and deficit at zenith and nadir, respectively; the effect is similar to the antenna being at a different height. The polarimetric antenna phase difference, $\Phi^{\mathrm{L-R}} = \Phi^{\mathrm{L}} - \Phi^{\mathrm{R}}$, evaluated across different polarizations and at the same viewing direction, is less well known and approximated here as -90 °.

Direct electric field

The direct electric field is expressed as:

$$\overline{E}_{\mathrm{d}} = \left[E_{\mathrm{d}}^{\mathrm{R}}, \quad E_{\mathrm{d}}^{\mathrm{L}} \right]^{\mathrm{T}} = \left(\sqrt{P_{\mathrm{d}}^{\mathrm{R}}}/L_{\mathrm{iso}}\right) \exp\left(\imath \phi_{\mathrm{d}}^{\mathrm{R}}\right) \left[1, \quad E_{\mathrm{d}}^{\mathrm{L/R}} \right]^{\mathrm{T}} \tag{25}$$

where $P_{\mathrm{d}}^{\mathrm{R}}/L_{\mathrm{iso}}^2$ (units $\mathrm{W/m^2}$) is the power spatial density. The direct polarimetric field ratio is $E_{\mathrm{d}}^{\mathrm{L/R}} = E_{\mathrm{d}}^{\mathrm{L}}/E_{\mathrm{d}}^{\mathrm{R}} = \sqrt{P_{\mathrm{d}}^{\mathrm{L/R}}} \exp\left(\imath \phi_{\mathrm{d}}^{\mathrm{L-R}}\right)$. The direct polarimetric power ratio,

$$P_{\mathrm{d}}^{\mathrm{L/R}} = \left(\frac{\alpha_{\mathrm{d}} - 1}{\alpha_{\mathrm{d}} + 1}\right)^2 = \beta_{\mathrm{d}}^2 \tag{26}$$

is related to the direct field polarization ellipticity as

$$\alpha_{\mathrm{d}} = \frac{\left|E_{\mathrm{d}}^{\mathrm{R}}\right| + \left|E_{\mathrm{d}}^{\mathrm{L}}\right|}{\left|E_{\mathrm{d}}^{\mathrm{R}}\right| - \left|E_{\mathrm{d}}^{\mathrm{L}}\right|} \tag{27}$$

Transmitted signal

The signals broadcast by GPS satellites are predominantly RHCP, with the LHCP magnitude specified never to exceed 20 % of the RHCP (ellipticity $\alpha_{\mathrm{d}} \leq 3.2$ dB [GPSW 2010]). It is important to recognize that, even at grazing incidence, the boresight angle at the transmitting GPS satellite antenna is only $\sim 13°$, subtended between the GPS orbital radius $\sim 26,000$ km and the earth radius $\sim 6,370$ km. So the approximation $P_{\mathrm{d}}^{\mathrm{L/R}} \approx 0$ typically remains accurate down to the lowest elevation angles. Under this assumption, the direct polarimetric electric field phase difference $\phi_{\mathrm{d}}^{\mathrm{L-R}} = \phi_{\mathrm{d}}^{\mathrm{L}} - \phi_{\mathrm{d}}^{\mathrm{R}}$ becomes irrelevant. This is fortunate because, despite the simulator allowing for the specification of $\phi_{\mathrm{d}}^{\mathrm{L-R}}$, this value depends on currently publicly unknown GPS satellite antenna radiation patterns, and also on the varying ionospheric conditions as the two circular polarizations propagate differently in nonisotropic media.

The various GPS frequency/code signal combinations have different specified received power levels, which shift the SNR decibel curves up and down. The satellite antenna gain patterns are not made available to the public, or else one could easily compute the expected power level based on the ephemeris-calculated satellite-receiver distance. In the lack of such ancillary information, we rely on the fact that satellite gain patterns were designed to compensate for the increased range, from satellite nadir to earth's limb (or from receiver's zenith to horizon), keeping the variations in received power level to within 2 dB. The power available for an isotropic antenna in GPS is typically $P_{\mathrm{d}}^{\mathrm{R}} \sim -160$ dB/W. More exact values as well as the remaining variation are specified in GPSD-USAF (2011) as a function of elevation angle and are incorporated in the simulator.

Reflected electric field

The reflected electric field is decomposed as $\overline{E}_{\mathrm{r}} = SD\overline{\overline{R}}\,\overline{E}_{\mathrm{d}}$. It is expressed in terms of the direct field $\overline{E}_{\mathrm{d}}$, incident on the receiving antenna, not the field incident on the surface. In the following, we explain the remaining components, in the order that they are applied to $\bar{E}_{\mathrm{d}}$.

Medium composition

The reflection matrix $\overline{\overline{R}} \in \mathbb{C}^{2\times 2}$,

$$\overline{\overline{R}} = R^{\mathrm{S}}\overline{\overline{P}}^{\mathrm{S}} + R^{\mathrm{X}}\overline{\overline{P}}^{\mathrm{X}} \tag{28}$$

is a combination of same- and cross-sense polarizing matrices, where $\overline{\overline{P}}^{\mathrm{S}}$ is the 2 by 2 identity matrix and $\overline{\overline{P}}^{\mathrm{X}} = \begin{bmatrix} 0 & 1 \\ 1 & 0 \end{bmatrix}$ is the first Pauli matrix. The circularly polarized scalar reflection coefficients are defined as:

$$R^{\mathrm{S}} = \left(R^{\mathrm{H}} + R^{\mathrm{V}}\right)/2 \tag{29}$$

$$R^{\mathrm{X}} = \left(R^{\mathrm{H}} - R^{\mathrm{V}}\right)/2 \tag{30}$$

The linearly polarized reflection coefficients follow from the solution of the Fresnel equations for two homogeneous halfspaces:

$$R^{\mathrm{H}} = (\varepsilon\cos\theta - \xi)/(\varepsilon\cos\theta + \xi) \tag{31}$$

$$R^{\mathrm{V}} = (\cos\theta - \xi)/(\cos\theta + \xi) \tag{32}$$

where $\xi = \sqrt{\left(\varepsilon - \sin^2\theta\right)}$; the angle of incidence (with respect to the surface normal) is denoted θ; the permittivity ratio, $\varepsilon = \varepsilon_{\mathrm{b}}/\varepsilon_{\mathrm{t}}$, relates bottom and top halfspaces. The top one ε_{t} can typically be assumed unity, for air, except when dealing with layered media. The bottom permittivity $\varepsilon_{\mathrm{b}} = \varepsilon'_{\mathrm{b}} + \imath\varepsilon''_{\mathrm{b}}$ is made of real and imaginary components, the latter of which can also be related to conductivity σ as

$$\varepsilon'' = \sigma/(2\pi f\varepsilon_0) \approx \sigma\lambda 60\ \mathrm{S}^{-1} \tag{33}$$

in terms of the carrier frequency f (in hertz); wavelength λ; a derived constant $60\ \mathrm{S}^{-1} \approx \mu_0 c_0/(2\pi)$, in units of reciprocal of Siemens; and vacuum constants: permittivity ε_0, permeability μ_0, and speed of light, c_0.

Interface geometry

The complex-valued scalar $I = |I|\exp(\imath\phi_I)$ has phase $\phi_I = k\tau_{\mathrm{i}}$, where $k = 2\pi/\lambda$ is the wavenumber and τ_{i} is the interferometric delay. For a planar horizontal surface, the latter is simply (Georgiadou and Kleusberg 1988):

$$\tau_{\mathrm{i}} = 2H\sin e_{\mathrm{d}} \tag{34}$$

in terms of the reflector height (height of the antenna above the ground), H, and the direct signal elevation angle e_{d} (with respect to the receiver local horizon). The interferometric delay rate, assuming a constant reflector height, is

$$\dot{\tau}_{\mathrm{i}} = 2H\dot{e}_{\mathrm{d}}\cos e_{\mathrm{d}} \tag{35}$$

Thus, for a constant elevation angle rate, $\dot{e}_{\mathrm{d}}$, the specular point travels faster at shallower incidence. Finally, under the assumption of a planar horizontal surface, the reflection elevation angle is trivially $e_{\mathrm{r}} = -e_{\mathrm{d}}$.

The magnitude is $|I| = 1$, which means that the additional propagation distance τ_{i} does not create a free-space propagation loss; this follows from the assumption of a plane incident wave and infinite planar interface. The sign of the propagation phase must be consistent with the sign of the imaginary component of permittivity, such that forward propagation in a lossy medium ($\Im\{\varepsilon\} > 0$) does indeed lead to power loss: $\lim_{\tau\to\infty}|\exp(\imath k\tau\sqrt{\varepsilon})| = 0$.

Random surface roughness

The magnitude $|S|$ represents a loss of coherent power. We calculate it from the theories of coherent scattering from random surfaces (Beckmann and Spizzichino 1963), as

$$|S| = \exp\left(-0.5k^2 s_{\mathrm{h}}^2\cos^2\theta\right) \tag{36}$$

where s_{h} is the surface height standard deviation (in meters); notice that it is polarization-independent. Random roughness has been reported to also have an effect on phase, ϕ_{S}, causing an apparent surface raise (diminished reflector height); this follows from the preferential illumination of surface crests, compared to shadowed surface troughs (Bourlier et al. 2006). Notice that the power effect is greatest at normal incidence, whereas the phase effect would be greatest at grazing incidence. Currently, the forward model only accounts for the magnitude effect, thus assuming $S = |S|$. Bourlier et al. (2006) state that the shadowing effect can be neglected for grazing angles greater than $\mathrm{atan}\left(2\sqrt{2}s_{\mathrm{h}'}\right)$, where $s_{\mathrm{h}'}$ is the standard deviation of surface slopes; users should be aware of this caveat, especially those dealing with dynamic surfaces, as in ocean scattering.

Noise power

In the GPS literature, it is customary to introduce the notation C for effective carrier power, which includes receiver losses absent in P_{c} as above; typically, these are power transmission losses between the antenna and the preamplifier (Spilker et al. 1996). Here, we neglect that, assuming instead $C = P_{\mathrm{c}}$. Carrier power becomes

combined with the noise power spectral density N_0 to form the carrier-to-noise density ratio, C/N_0 (in hertz); and with the noise bandwidth, B_n, to form the carrier-to-noise ratio, C/P_n (in watts per watt) via the noise power $P_n = N_0 B_n / K$ modified by a unitless factor K defined below. The RINEX "S" observables are thus taken here as $\mathrm{SNR} = C/P_n$.

Noise density $N_0 = k_B T$ is calculated as the product of the Boltzmann constant, $k_B \approx 1.38 \times 10^{-23}\,\mathrm{J/K}$, and a noise-equivalent temperature, $T = T_A + T_R$. The antenna contribution T_A lies in the range 75–130 K for a typical installation and hemispherical gain (Langley 1997), and reaches a much higher ambient temperature ($\sim$290 K) when the antenna is replaced by a hardware simulator. The receiver contribution is taken as $T_R \approx 470\,\mathrm{K}$, corresponding to a circuit made of a low-noise amplifier in between a short and long cables, connecting the antenna element to the receiver (Misra and Enge 2006). Both values depend on the installation, i.e., whether the antenna is upright, the length and physical temperature of the cables, etc. The noise density is the same for all satellites tracked at the same time with the same antenna, but it does vary over time.

The modified noise power as P_n includes a nonnegative factor K representing tracking losses, mainly related to the code modulation, which can be quite severe and disfigure the multipath modulation otherwise clearly present in SNR. These are, for example, codeless tracking losses affecting the encrypted P(Y) codes (Woo 2000) and cross-channel self-interference (i.e., between different satellites), which significantly impact the shorter C/A codes (Lestarquit and Nouvel 2012). For the newer L2C code, K can be neglected without degradation in the model/observation agreement; this is because these codes, contrary to the P(Y), are publicly known; and in contrast to C/A, they are sufficiently long (Fontana et al. 2001).

Simplified expressions

The rigorous forward model exposed above relies on matrix/vector operations. Alternatively, we can write the resulting direct and reflected powers in full assuming a purely RHCP incident electric field:

$$P_d = P_d^R G_d^R W_d^2 \tag{37}$$

$$P_r = P_d^R |XSW_r|^2 \tag{38}$$

Notice that the isotropic antenna complex effective length L_{iso} cancels out. This assumption—which can be disabled in the simulator, but without which the mathematical formulae quickly become unyielding—allows us to interpret the same-polarization reflection coefficient as RHCP producing, and similarly for LHCP/cross-polarization. We can further define coupled surface/antenna coefficients,

$$X^R = R^S \sqrt{G_r^R} \exp\left(\imath \Phi_r^R\right) \tag{39}$$

$$X^L = R^X \sqrt{G_r^L} \exp\left(\imath \Phi_r^L\right) \tag{40}$$

as well as their complex sum, $X = X^R + X^L$. The interferometric phase then reads

$$\phi_i = \phi_X + \phi_I - \Phi_d^R \tag{41}$$

The first term $\phi_X = \arg(X)$ accounts for the surface and antenna effects on the reflection; the second one $\phi_I = k\tau_i$ follows from the interferometric propagation delay; the third one Φ_d^R is the antenna phase contribution to the direct voltage. These are the terms not in common between the direct and reflected voltage phases:

$$\phi_d = \phi_d^R + \Phi_d^R \tag{42}$$

$$\phi_r = \phi_d^R + \phi_X + \phi_I \tag{43}$$

As the direct electric field phase ϕ_d^R cancels out of the interferometric phase $\phi_i = \phi_r - \phi_d$, it can be safely ignored in multipath modeling; this is tremendously useful, because we need not consider clock errors, atmospheric propagation delays—at least the bulk of it, especially for near-surface antennas—and other effects that would otherwise need to be accounted for in a positioning solution. Final SNR observations $\mathrm{SNR} = \mathrm{tSNR} + \mathrm{dSNR}$ are then the sum of a trend:

$$\mathrm{tSNR} = \left(P_d + P_r + P_r^I\right) P_n^{-1} \tag{44}$$

and detrended interference fringes:

$$\mathrm{dSNR} = 2\sqrt{P_d}\sqrt{P_r P_n^{-1}} \cos \phi_i \tag{45}$$

Simulations

We now illustrate the main features of the forward model. We begin with simulations for a typical scenario found at geodetic installations. We proceed to explore the various GPS transmitted signals. It is followed by an exploration of the surface characteristics. We finish up considering the impact of the antenna setup—its height above the ground, orientation, and gain pattern. The implications for positioning and reflectometry applications are emphasized.

Nominal conditions

We assume a horizontal ground surface, made up of soil with medium-level moisture and negligible roughness, observed with a choke-ring antenna installed upright on a 1.5 m tall monument. Figure 1 shows the model results for the L2C signal observables: SNR, carrier phase multipath error, and pseudorange code multipath error, where error means the difference with respect to multipath-free

conditions. As one would expect, carrier phase multipath error is at least an order of magnitude smaller than the pseudorange multipath error and is limited to a quarter of wavelength provided the magnitude of the direct voltage remains greater than the reflected one (this condition can be violated in the presence of multiple reflections). Besides the rigorous solution, in the same figure, we show also results from the small-magnitude and small-delay approximations, Eqs. (5), (17), and (18).

All three observables exhibit a series of peaks and troughs, or fringes. Noticeable features in the interference patterns are the spacing between fringes, the horizontal position of the pattern as a whole, and magnitude variations. Although none of the observables is perfectly sinusoidal, a sinusoid can still be fit after some manipulation of the data. This fitting serves to quantify the multipath modulation frequency, phase shift, and amplitude. In a variety of cases, the best-fitting sinusoid parameters can be related to physical properties describing the environmental conditions in the antenna surroundings. For linearly polarized antennas, the multipath effect requires a different fitting procedure (Rodriguez-Alvarez et al. 2011b).

Figure 2 shows the constituting quantities responsible for producing the observables presented in Fig. 1. The top panel demonstrates how interferometric power P_{i} is direction-dependent, increasing with decreasing elevation angle, as the direct and reflected power converge. This violation in the common assumption $P_{\mathrm{r}} \ll P_{\mathrm{d}}$ follows from the surface/antenna polarization matching, as detailed below. The bottom panel separates the geometrical ϕ_I and compositional ϕ_X components of the interferometric phase ϕ_{i}, which depend on the propagation delay and surface material, respectively. The former is a linear function of sine of elevation angle, $\tau_{\mathrm{i}} = 2H \sin e$, whereas the latter is a more complicated sigmoid-like function (it would be essentially a constant for a metallic surface). It should be highlighted that the complicated oscillations present in error power and phase follow from simpler monotone variations in the underlying interferometric quantities. Consequently, interferometric parameters could be more tightly constrained than error parameters if using measurements to model multipath.

Reflector height

Changing the height of the antenna above the ground or reflecting surface changes primarily the modulation frequency and phase shift (Fig. 3). This is caused by the interferometric delay. For a horizontal surface, the specular point gets closer to the antenna with decreasing reflector height, yet the incident and reflection directions remain the same. Consequently, there are no changes in the surface/antenna response, which is function of the incident and reflection angles. The only change in the modulation amplitude is caused by the code modulation, which decreases the reflected power with increasing delay, although it would only be significant for very large reflector heights.

The ideal reflector height depends on the purpose of the application. For example, one might situate an antenna differently for reference frame realization versus real-time deformation monitoring. In the latter application, high-rate

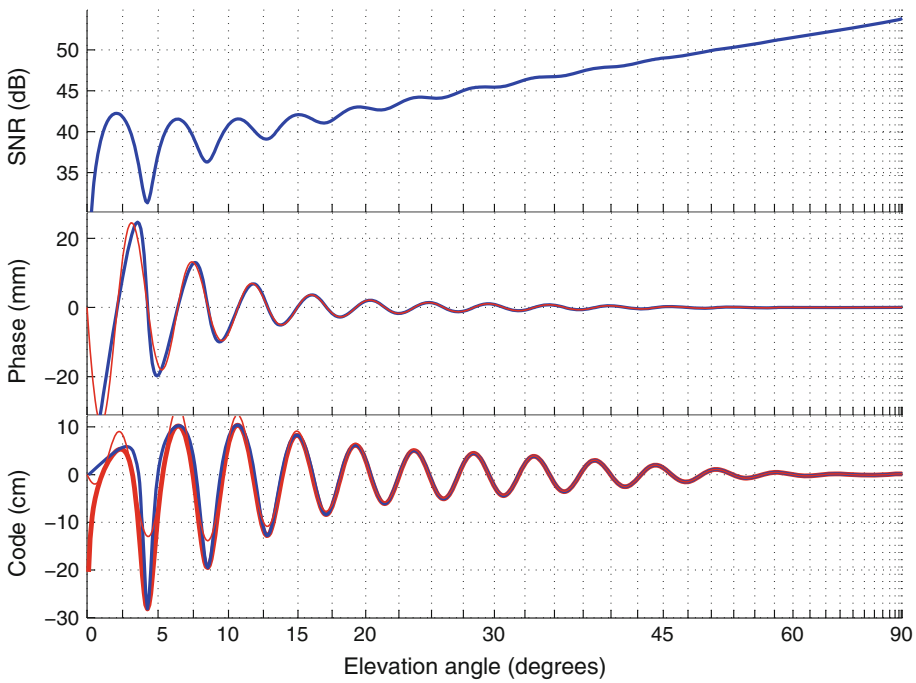

Fig. 1 Multipath signature in GPS SNR, carrier phase, and code pseudorange observables for a typical setup. The reflecting surface is horizontal, made up of soil with medium-level moisture and negligible roughness. A choke-ring antenna installed upright on a 1.5-m-tall monument is postulated. The rigorous solution is shown in *blue*, approximations in *red*; for code pseudorange, the thick (thin) *red line* corresponds to small-delay (small-delay and small-power) approximation. Please notice the difference in *scales* between code (cm) and phase (mm)

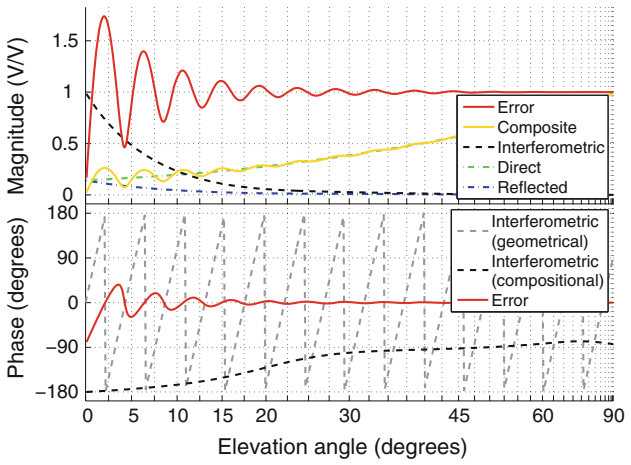

Fig. 2 Magnitude and phase of modeled signals. *Top panel* reflected, direct, interferometric, composite, and error magnitudes; *bottom panel*: interferometric and error phases. These are the underlying constituting quantities responsible for producing the observable signatures presented in Fig. 1

displacements are the quantity of interest, so an antenna closer to the ground would introduce fewer artifacts in the position time series. For a reference frame site, absolute position biases are to be avoided, so a taller antenna would seem preferable, because multipath errors would more likely average to zero. Although code pseudorange RMS error increases without bound in proportion to reflector height, carrier phase observations are more important for long static positioning sessions. For reflectometry, taller antennas are preferred; for example, for snow sensing, the antenna should be built much taller (more than two wavelengths) than the highest expected snow level.

Random surface roughness

The surface height standard deviation s_h serves as a parameterization for loss of coherent power (recall that we have incorporated coherence into the reflection voltage). Various phenomena other than random surface roughness can cause loss of coherence, from clock dither, to atmospheric turbulence, and volumetric inhomogeneities. Thus, care needs to be exercised in interpreting s_h as an effective parameter or equivalent roughness, an amalgamation of different sources affecting coherently reflected power.

Degree of coherence reduction will decrease the visibility of interference fringes. For example, in optical interferometry, intensity fringes become fainter; in radar imaging, phase fringes become noisier. In GPS, SNR multipath modulation amplitude decreases; if we could measure the interferometric phase directly, it would be noisier but its mean value would be unaffected. In contrast, the error phase would predominantly diminish in magnitude because it also involves the (coherent) interferometric power, $\phi_e \approx \sqrt{P_i} \sin \phi_i$.

In this forward model, we account explicitly only for loss of coherence due to surface random roughness, which is driven by a single free parameter, surface height standard deviation (with respect to a trend surface, possibly

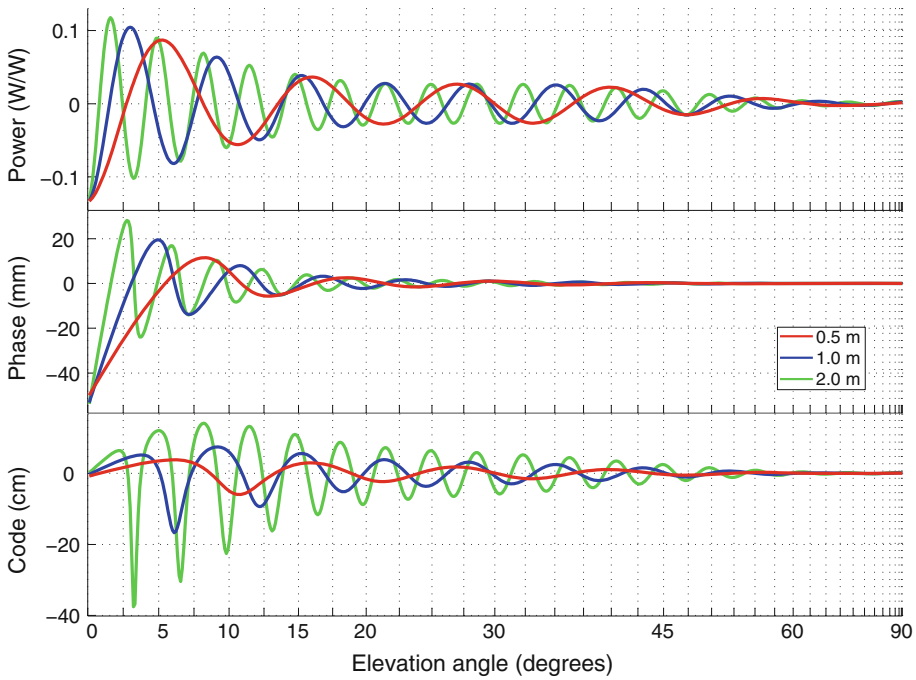

Fig. 3 Effect of reflector height on GPS multipath errors. Reflector height values equal to 1/2, 1, and 2 m are shown in *red*, *blue*, and *green*, respectively

undulated). Notice that height correlation length does not directly affect the coherent power, although the former is assumed to be much smaller than the illuminated portion of the surface (so that several roughness cycles contribute to the reflection). The average of surface deviations, or trend surface, does not suffer randomization during the coherent integration period and would require a deterministic rather than stochastic model (not covered here).

Increasing surface roughness decreases the magnitude of the multipath modulation in all three GPS observables (Fig. 4), and it does so in an elevation angle dependent manner: higher/lower elevation observations are more/less affected by roughness. Consequently, installing a geodetic monument in a site where the antenna is surrounded by randomly shaped objects, e.g., rocks, would be a valid multipath mitigation strategy. The efficiency would depend on the size of objects, although they would not need to be made of radiofrequency-absorbing material, or metal, or have any other specific composition. Vegetation plays a similar role. For the same reason that surface roughness is benign for positioning applications, it represents a fundamental physical limit for coherent reflectometry, as it may extinguish the multipath modulation and thus the environmental retrieval.

Surface material

The material composition—types (water, concrete, soil, etc.) and their properties (soil moisture, snow density, etc.)—has an impact on all aspects of the multipath modulation (Fig. 5). The medium is modeled as an effective homogeneous material with an equivalent complex-valued permittivity, which is input into the conventional Fresnel reflection formulae.

Each material produces different GPS observations, not just directly through the Fresnel reflection coefficients themselves, but also because they elicit a different response from the antenna, depending on the reflection polarization. Two polarization regimes are demarcated by the Brewster angle, separating LHEP reflections (left-handed elliptically polarized) at higher elevation angles from RHEP at lower angles. The Brewster angle is lowered by the medium conductivity, e.g., it is about 10 degrees for wet ground versus $\sim 25^\circ$ for dry ground (Fig. 6).

Although a metal surface yields a strong reflected electric field, it results in a weak reflected voltage as the LHEP field is captured by a RHEP antenna. Reflections off dielectric media, such as most natural land surfaces, retain the polarization of the incident vector electric field in the limit of grazing incidence. In this case, the antenna will receive the reflected field with nearly as much gain as the direct field.

Antenna pattern

GPS antennas for positioning applications are typically installed upright (boresight facing zenith). The RHCP gain

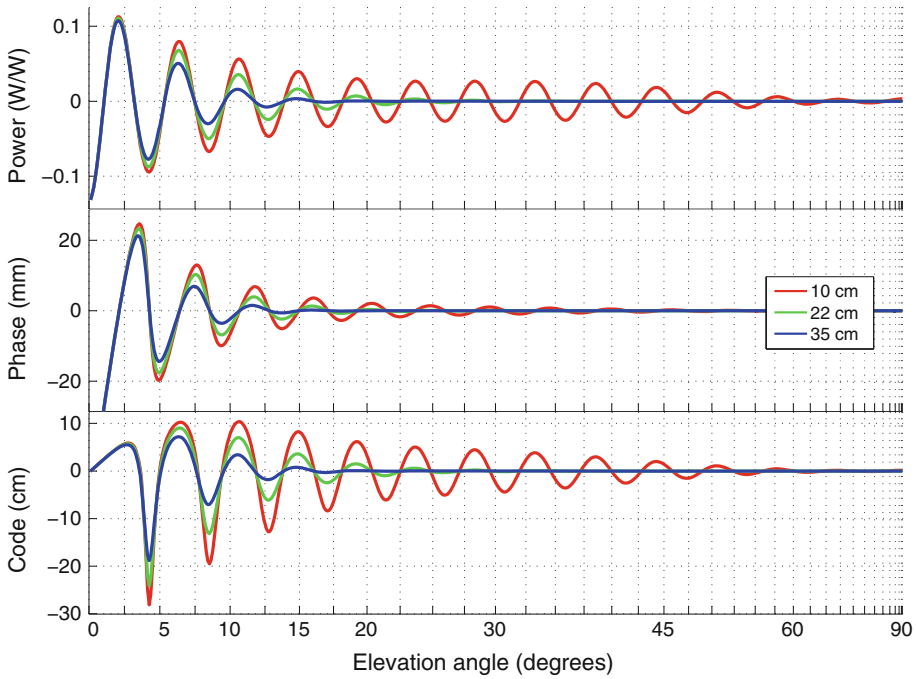

Fig. 4 Effect of surface random roughness on GPS multipath errors. Surface height standard deviation values equal to 0, 25, and 35 cm are shown in *red*, *green*, and *blue*, respectively

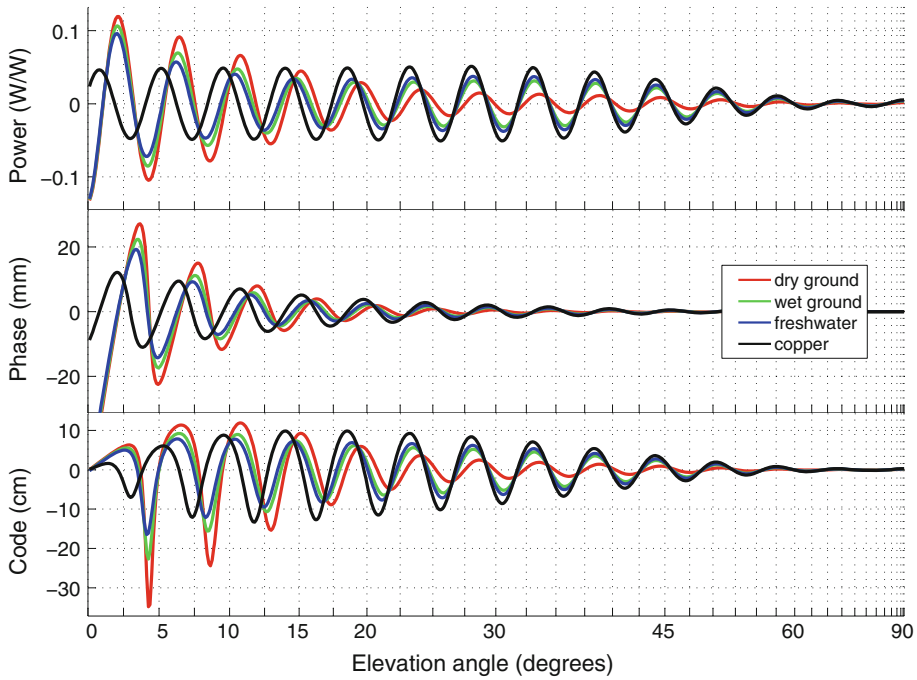

Fig. 5 Effect of surface material composition on GPS multipath errors

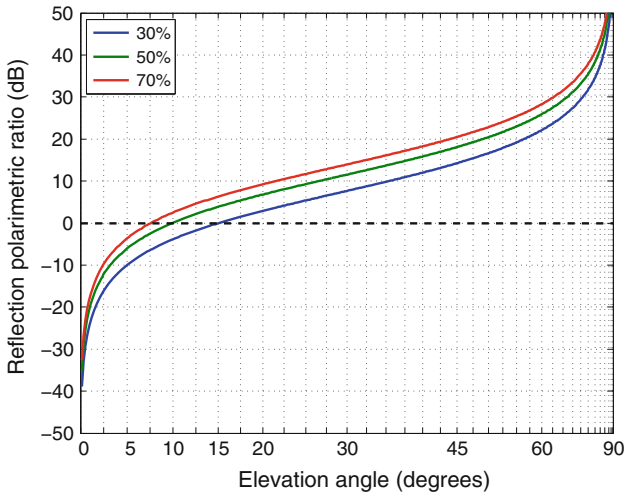

Fig. 6 Effect of soil moisture on reflection polarimetric ratio for varying volumetric water content. The Brewster angle is found at the intersection with the *horizontal line* at 0 dB

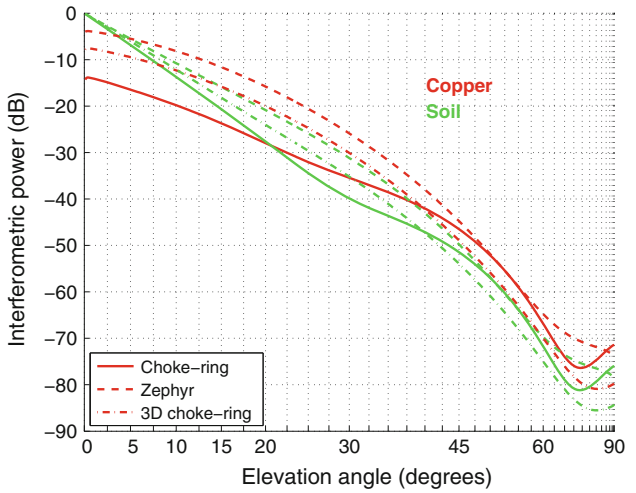

Fig. 7 Effect of antenna model on interferometric power. Combinations of two surface materials and three geodetic-quality antenna models are compared. Soil is shown in *green*, copper in *red*; choke-ring, zephyr, and 3D choke-ring (IGS antenna codes TRM29659.00, TRM55971.00, and LEIAR25) are shown, respectively, in *solid*, *dashed*, and *dash-dot line* styles. L1 and C/A are assumed for the carrier frequency and code modulation

pattern is very much omni-directional in azimuth and quasi-hemispherical in elevation angle. The LHCP gain pattern is not as well defined, except that near boresight, it is much smaller than RHCP (by $\sim$20 dB); in the antenna anti-boresight direction, there are alternating regions where RHCP and LHCP predominate.

Comparing different geodetic antennas (Fig. 7), there is no significant difference in the interferometric power (i.e., reflected over direct) for a soil surface. It is only for metallic surfaces that the classic choke-ring design outperforms the other antennas in terms of multipath mitigation (Fig. 8). Interestingly, a metallic horizontal surface appears less harmful than bare ground at near-grazing incidence, since geodetic-quality antennas are designed to reject LHCP reflections, but offer little impediment for RHCP intake.

The antenna phase pattern may also impact multipath. At RHCP, this effect is at about the millimeter level for

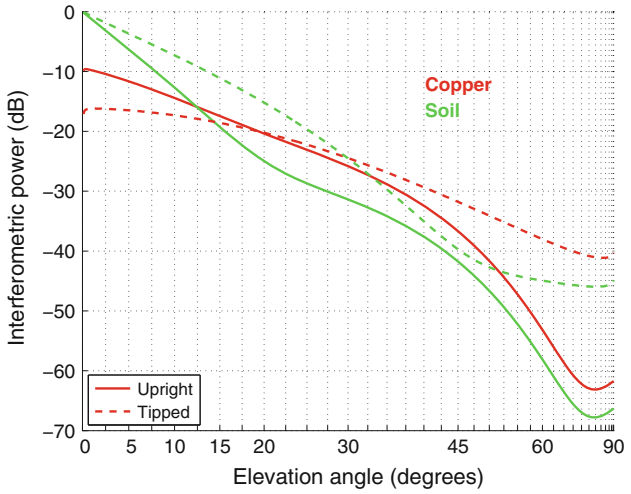

Fig. 8 Effect of antenna orientation on interferometric power. Combinations of two surface materials and two antenna orientations are compared. Soil is shown in *green*, copper in *red*; upright and tipped orientations are shown, respectively, in *solid* and *dashed line* styles

geodetic antennas, and thus usually negligible. The phase difference across different polarizations at the same viewing direction is approximated here as $-90°$, as discussed in Zavorotny et al. (2010). This has a greater impact for normal incidence or conducting surfaces, which produce predominantly LHCP reflections. It is crucial for replicating the change in SNR modulation phase observed between dry and wet soil conditions. The LHCP phase pattern needs better characterization in the future.

Antenna orientation

For positioning applications, the ideal antenna installation is upright (zenith-looking). However, some reflectometry studies tip the antenna (boresight facing the horizon) or have it upside-down (nadir-looking). The main advantage is the improved reception of reflections. These special orientations require a dedicated installation, in contrast to the upright configuration, which allows the GPS unit to be shared with geodesists, surveyors, and atmospheric scientists.

Changing the antenna orientation also allows neglecting polarization diversity under certain circumstances. For example, with a tipped antenna and low-elevation satellite, the LHCP reflection is suppressed; with an upside-down antenna and a high-elevation satellite, the RHCP component is suppressed. Another simplification offered by tipped installations is that the antenna subjects like-polarized direct and reflected fields to practically the same response (Treuhaft et al. 2001). A tipped antenna installation (Rodriguez-Alvarez et al. 2011a) is also advantageous when using shorter code modulations, such as C/A, because it reduces the cross-channel self-interference (as the maximum gain is applied to the rising or setting satellite being pointed at, rather than to a different high-elevation satellite simultaneously in view). The main drawback of tipping the antenna is the loss of visibility to satellites in azimuths far from boresight, which is a missed opportunity for more frequent retrievals.

Other times, a more drastic configuration is chosen, with the goal of measuring only the reflection, e.g., an LHEP

Fig. 9 Multipath signature in GPS SNR, carrier phase, and code pseudorange observables for an atypical setup. An LHCP-predominant antenna is installed upside-down, 1.5 m above seawater. Results for varying surface random roughness are shown in *red*, *green*, and *blue*, corresponding to surface height standard deviation values of 0, 7.1, and 10.0 cm, respectively. L1 and C/A are assumed for the carrier frequency and code modulation

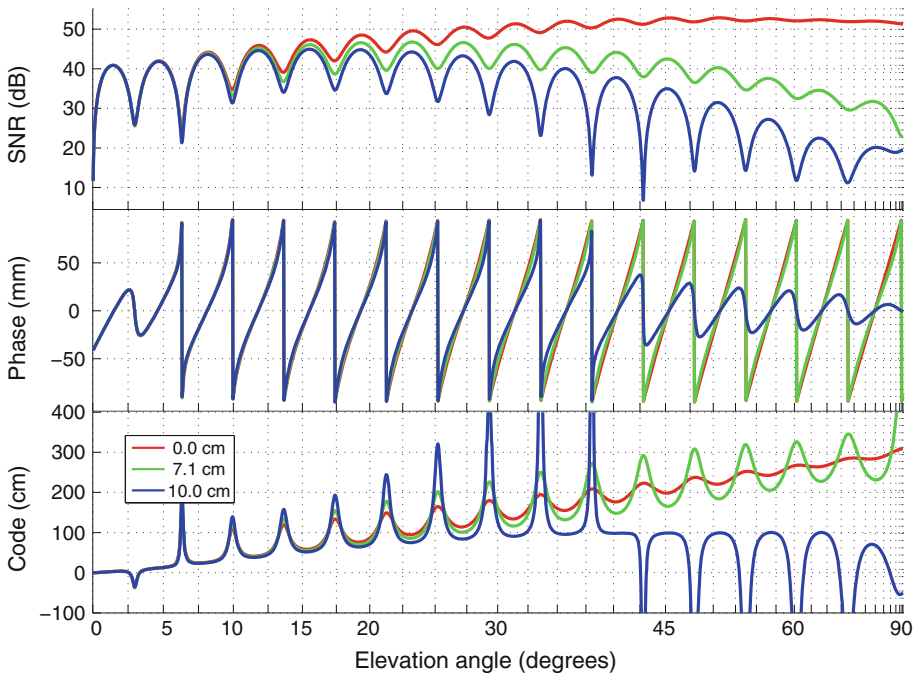

antenna (i.e., predominantly LHCP) is installed upside-down (Löfgren et al. 2011) (Fig. 9). In this case, the absence of interference fringes is caused by a weak direct voltage, not a weak reflection. The carrier phase and pseudorange multipath errors are essentially the respective interferometric quantities. The delay error reaches twice the reflector height (1.5 m) at zenith; phase error exceeds 90°—and in fact wraps around the 19 cm wavelength, as intended.

Conclusions

We have presented a forward model for GPS terrestrial multipath—i.e., reflections off land, water, etc.—as experienced by near-surface receivers. It produces GPS carrier phase, pseudorange, and SNR observables, combining different surface and antenna types, with due consideration for electromagnetic polarization and coherence. The forward model requires a priori information about the parameters affecting the amount of attenuation as well as group and phase delay exhibited by reflections, compared to the direct or LOS signal:

- properties of target surface (geometry and composition),
- measurement system characteristics (code modulation, receiver tracking algorithms, antenna radiation patterns), and
- monitoring setup (height of the antenna above the ground, as well as its orientation).

Starting from the direct and reflected voltages, we have defined and related the interferometric, error, and composite voltages. We presented and discussed a number of situations, based on which we have drawn conclusions useful for the design and analysis of reflectometry experiments. For instance, we considered how the antenna orientation—upright, tipped, or upside-down,— involves a number of trade-offs, regarding the neglect of the antenna gain pattern, the minimization of CDMA self-interference, and the maximization of the number of satellites visible. This forward model was also used to understand the multipath signature in GPS positioning applications. For example, we have shown how geodetic GPS antennas offer little impediment for the intake of near-grazing reflections off natural surfaces (in contrast to off metal), because of the lack of diversity with respect to the direct signal, i.e., small interferometric delay and Doppler, such as sense of polarization, and similar direction of arrival.

Acknowledgments This research was supported by NSF (EAR 0948957, AGS 0935725). Mr. Nievinski has been supported by a Capes/Fulbright Graduate Student Fellowship and a NASA Earth System Science Research Fellowship. Reviewers and the editor are gratefully acknowledged for their comments.

References

Beckmann P, Spizzichino A (1963) The scattering of electromagnetic waves from rough surfaces. Pergamon (Republished by Artech, 1987), p 503

Bourlier C, Pinel N, Fabbro V (2006) Illuminated height PDF of a random rough surface and its impact on the forward propagation above oceans at grazing angles. 2006 First European Conference on Antennas and Propagation. IEEE, pp 1–6. doi:10.1109/EUCAP.2006.4584894

Fontana RD, Cheung W, Novak PM, Stansell TA (2001) The new L2 civil signal. Proc ION GPS. Institute of Navigation, Salt Lake City, pp 617–631

Georgiadou Y, Kleusberg A (1988) On carrier signal multipath effects in relative GPS positioning. Manuscr Geodaet 12:172–179

GPSD-USAF (2011) Navstar GPS space segment/navigation user segment interfaces, Revision F (IS-GPS-200F). p 210

Langley RB (1997) GPS receiver system noise. GPS World 8:40–45

Larson KM, Small EE, Gutmann ED, Bilich AL, Braun JJ, Zavorotny VU (2008) Use of GPS receivers as a soil moisture network for water cycle studies. Geophys Res Lett 35:L24405. doi:10.1029/2008GL036013

Larson KM, Gutmann ED, Zavorotny VU, Braun JJ, Williams MW, Nievinski FG (2009) Can we measure snow depth with GPS receivers? Geophys Res Lett 36:L17502. doi:10.1029/2009GL039430

Lestarquit L, Nouvel O (2012) Determining and measuring the true impact of C/A code cross-correlation on tracking—application to SBAS georanging. Proc IEEE/ION PLANS. IEEE, pp 1134–1140. doi:10.1109/PLANS.2012.6236968

Löfgren JS, Haas R, Scherneck H-G, Bos MS (2011) Three months of local sea level derived from reflected GNSS signals. Radio Sci 46:1–12. doi:10.1029/2011RS004693

Milligan TA (2005) Modern antenna design. Wiley-IEEE, New Jersey, p 632

Misra P, Enge P (2006) Global positioning system: signals, measurements, and performance, 2nd ed. Ganga-Jamuna, p 569

Rodriguez-Alvarez N, Bosch-Lluis X, Camps A, Aguasca A, Vall-llossera M, Valencia E, Ramos-Perez I, Park H (2011a) Review of crop growth and soil moisture monitoring from a ground-based instrument implementing the interference pattern GNSS-R technique. Radio Sci 46:1–11. doi:10.1029/2011RS004680

Rodriguez-Alvarez N, Camps A, Vall-llossera M, Bosch-Lluis X, Monerris A, Ramos-Perez I, Valencia E, Marchan-Hernandez JF, Martinez-Fernandez J, Baroncini-Turricchia G, Perez-Gutierrez C, Sanchez N (2011b) Land geophysical parameters retrieval using the interference pattern GNSS-R technique. IEEE Trans Geosci Remote Sens 49:71–84. doi:10.1109/TGRS.2010.2049023

Small EE, Larson KM, Braun JJ (2010) Sensing vegetation growth with reflected GPS signals. Geophys Res Lett 37:L12401. doi:10.1029/2010GL042951

Spilker JJ, Enge PK, Parkinson BW, Axelrad P (1996) Global positioning system: theory and applications. AIAA, p 781

Treuhaft RN, Lowe ST, Zuffada C, Chao Y (2001) 2-cm GPS altimetry over Crater Lake. Geophys Res Lett 28:4343. doi:10.1029/2001GL013815

Woo KT (2000) Optimum semicodeless carrier-phase tracking of L2. Navig 47:82–99

Zavorotny VU, Voronovich AG (2000) Scattering of GPS signals from the ocean with wind remote sensing application. IEEE Trans Geosci Remote Sens 38:951–964. doi:10.1109/36.841977

Zavorotny VU, Larson KM, Braun JJ, Small EE, Gutmann ED, Bilich AL (2010) A physical model for GPS multipath caused by land reflections: toward bare soil moisture retrievals. IEEE J Sel

Topics Appl Earth Observ 3:100–110. doi:10.1109/JSTARS.2009.2033608

Author Biographies

Felipe G. Nievinski is a postdoctoral researcher at UNESP, Brazil, where he works in the field of GPS multipath reflectometry. He earned his PhD (Aerospace) from the University of Colorado Boulder in 2013, M.Sc.E. (Geodesy) from the University of New Brunswick in 2009, and B.E. (Geomatics) from UFRGS, Brazil, in 2005.

Kristine M. Larson is a Professor of Aerospace Engineering Sciences at the University of Colorado. Her current research focuses on GPS reflections.